Appl Phys B (2010) 99: 299–306
DOI 10.1007/s00340-009-3793-4

Applied Physics B
Lasers and Optics

Transport of high-fluence energy by femtosecond filament in air

V.Y. Fedorov · O.V. Tverskoy · V.P. Kandidov

Received: 8 July 2009 / Revised version: 25 September 2009 / Published online: 1 November 2009

Abstract We present a numerical investigation of high-fluence energy transport by a femtosecond filament in air. Our study shows that an increase of the initial pulse duration leads to an increase of this energy in the pulse and to its higher localization in the filament.

PACS 42.65.Jx · 42.68.Ay

1 Introduction

During filamentation of a femtosecond laser pulse, energy localizes in both space and time. This localization is conserved on tens and hundreds of meters. Self-channeling of laser energy in a filament is a result of dynamical equilibrium between Kerr self-focusing and defocusing in induced laser plasma. This equilibrium can be reached under conditions of high power and short duration of the pulse. Spatio-temporal localization of energy during pulse filamentation is accompanied by plasma channel generation, generation of supercontinuum, and conical emission [1–3]. These features open fundamentally new possibilities for femtosecond laser technologies in atmospheric optics [4–6].

In air, the intensity in a filament is about 5×10^{13} W/cm^2 [7]. Such intensity leads to ionization of molecules of air gaseous components and to generation of plasma at the surfaces of ranged targets [6]. The method of filament-induced fluorescence spectroscopy (FIFS) was used for remote sensing of methane and ethanol molecules as well as other gaseous pollutants in air [8], bioaerosols consisting of riboflavin [9], and different salts [10]. Beam squeezing [11] and geometrical focusing [12] were used to increase the fluorescence signal, since they provide greater volume of nonlinear optical interaction of a light field with a medium.

The fluence inside the filament is high enough for ablation of metals [13] and optical breakdown of transparent dielectrics [14]. Thus, filaments of femtosecond laser pulses are promising tools for energy delivery and generation of a laser-induced plasma on remote objects. This is the basis for remote filament-induced breakdown spectroscopy (FIBS) [6].

The maximum remote sensing distance of a metallic target in the FIBS method was 90 m [13, 15]. According to estimations [16], in the FIBS method it is possible to obtain with one pulse a signal sufficient for diagnostics of metallic targets located at distances up to 1 km, and with lower spectral resolution—up to several kilometers. Experiments [13] showed that the signal from a target is maximal if the filaments were created several meters before the target surface. The authors note that in this case high fluence inside the filament initiates and sustains optical breakdown on a target surface during the whole pulse length.

Laser ablation or optical breakdown of a remote target occurs when the pulse fluence exceeds a certain threshold typical of a given condensed matter. Emission of plasma on the target (and therefore the received signal) is determined by the total amount of high-fluence energy (HFE) that is carried by the filament. The high-fluence energy can be determined as the energy for which the fluence is higher than the threshold one for a given sample.

V.Y. Fedorov (✉) · O.V. Tverskoy · V.P. Kandidov
International Laser Center and Faculty of Physics,
M.V. Lomonosov Moscow State University, Leninskie Gori,
Moscow 119991, Russia
e-mail: fedoroff_v@mail.ru
Fax: +7-495-9393113

In the present work we use numerical simulation to study transport of HFE by a femtosecond filament in air, and the influence of pulse duration on this process.

2 Formulation of the problem

In order to study energy characteristics of a femtosecond filament we performed numerical simulation of the femtosecond pulse propagation in air. Assuming that pulse propagation occurs along the z axis, the equation for the slowly varying envelope of the light field is [17, 18]

$$2ik_0\frac{\partial E}{\partial z} = \Delta_\perp E + k_0k_2\frac{\partial^2 E}{\partial t^2} + \frac{k_0}{2n_0}(\Delta n_k + \Delta n_\mathrm{p})E + i\alpha E, \quad (1)$$

where k_0 is the wave number and n_0 is the linear refractive index. The first term on the right-hand side of (1) describes diffraction, the second the dispersion in second-order approximation, and the third the contribution of Kerr and plasma nonlinearities. The last term corresponds to the absorption of radiation due to medium ionization.

Equation (1) does not contain an operator of self-steepening [19], which appears if we keep more terms in the time-variable expansion [20]. This operator allows one to describe an increase in the steepness of the pulse edges. This is essential in the study of pulse spectrum transformation. But, for analysis of energetic characteristics, the influence of self-steepening as well as higher-order dispersion is negligible.

The Kerr increment of the refractive index in air Δn_k is determined by electronic nonlinearity and induced Raman scattering on rotational transitions of air molecules, which lead to delayed nonlinear response [21]. The response time of Raman scattering in air is about 70 fs [22, 23] and it should be taken into account for pulses of femtosecond duration. According to [18, 24], for an increment Δn_k in air the following approximation is valid:

$$\Delta n_k = \frac{1}{2}n_2 I + \frac{1}{2}n_2\int_{-\infty}^{t} H(t-\tau)I(\tau)\,\mathrm{d}\tau, \quad (2)$$

where $H(t)$ is the response function; $I = c_0n_0\varepsilon_0|E|^2/2$ is the field intensity; and n_2 is the nonlinear coefficient of air. For air and wavelength 800 nm we used a nonlinear coefficient equal to $n_2 = 4\times10^{-19}$ cm^2/W, which corresponds to a self-focusing critical power of 2.4 GW.

The plasma contribution to the refractive index Δn_p is negative. In air, Δn_p is determined by the equation

$$\Delta n_\mathrm{p} = -\frac{1}{2n_0}\frac{\omega_\mathrm{p}^2}{\omega_0^2}, \quad (3)$$

where $\omega_\mathrm{p} = (e^2N_\mathrm{e}/m_\mathrm{e}\varepsilon_0)^{1/2}$ is the plasma frequency; e and m_e are the electron charge and mass; and N_e is the density of free electrons.

We considered air as a two-component medium consisting of 78% of nitrogen and 22% of oxygen. For each component, the density of free electrons $N_\mathrm{e}(r,z,t)$ is described by the equation

$$\frac{\partial N_\mathrm{e}}{\partial t} = R(I)(N_0 - N_\mathrm{e}), \quad (4)$$

where $R(I)$ and N_0 are the ionization rate and density of neutrals. In air of atmospheric pressure, the density of neutral molecules N_0 is small and the contributions of avalanche ionization and recombination are negligible. For the ionization rate $R(I)$ we used the Perelomov–Popov–Terent'ev model [25], which reproduces experimental data in a most adequate way [26].

In order to study filamentation, we solved numerically (1) in the approximation of axial symmetry. The initial pulse was collimated and had a Gaussian shape of its envelope in time and space:

$$E(x,y,t,z=0) = E_0\exp\left(-\frac{r^2}{2a_0^2}\right)\exp\left(-\frac{t^2}{2\tau_0^2}\right), \quad (5)$$

where E_0 is the initial amplitude; a_0 and τ_0 are the beam radius and half of the pulse duration at the e^{-1} level.

3 High-fluence energy in pulses with different duration

In order to study transport of HFE by a filament, we considered transform-limited pulses of 800-nm wavelength with constant energy $W_0 = 8$ mJ and beam radius $a_0 = 1.2$ mm. The full pulse duration $2\tau_0$ was varied from 100 fs to 2 ps. As long as the pulse energy is constant, an increase of pulse duration $2\tau_0$ results in a decrease of initial pulse intensity I_0 from 2×10^{12} for $2\tau_0 = 100$ fs to 10^{11} W/cm^2 for $2\tau_0 = 2$ ps. Correspondingly, the initial pulse power P_0 decreases from 90 GW to 4.5 GW, and the ratio of P_0 to the self-focusing critical power P_cr in air decreases from 38 to 1.9. Note that in the case of high P_0/P_cr ratio, multifilamentation takes place [27] and the regime of one filament is hypothetical.

Also, one should note that the beam radius we chose is less than the one which is usually used in experiments on realistic atmospheric paths. Our choice is determined by limitations of computer simulation. For a beam with 1.2-mm radius we can simulate filamentation with multiple refocusing, which determines the efficiency of HFE transport. We carried out analysis of transform-limited pulses with different durations in order to exclude the influence of their compression on the process of HFE transport. An example of HFE

transport by a chirped pulse is presented at the end of this section.

By solving (1)–(4) with the initial condition determined by (5) we determine the spatio-temporal evolution of the light field envelope $E(r,t,z)$ and the distribution of electron density $N_e(r,t,z)$ during pulse propagation. Further processing of these results allows us to derive parameters of the laser pulse and plasma channel, which one measures in experiments. For example, at given distance z the fluence distribution in the pulse cross section $F(r,z)$ is equal to

$$F(r,z) = \int I(r,t,z)\,\mathrm{d}t. \tag{6}$$

In order to introduce the HFE value we need to specify the threshold fluence F_{th} for plasma generation on a remote target. In general, the value of F_{th} depends on material properties, laser wavelength, and pulse duration. The mechanism of laser energy absorption is different for opaque and transparent samples. Linear absorption is the main contribution in opaque materials (e.g. metals), whereas absorption has to be realized by nonlinear processes of avalanche and multiphoton ionization in transparent materials (e.g. glass) [28]. Due to that, in general the threshold fluence F_{th} is higher for transparent materials. For example, for sub-picosecond laser pulse durations and for the wavelength of a Ti:sapphire laser, the threshold fluence for a copper sample is 0.12 J/cm^2 [29] and for fused silica is 1.5 J/cm^2 [30]. However, in the context of FIBS, the parameter of crucial interest is the threshold fluence for which the useful spectral lines emerge from the background signal. The existence of these lines implies that a plasma has been formed, so that one naturally expects this threshold to be significantly higher than the ablation or optical breakdown threshold. For example, in an experiment [31] the threshold fluence for the appearance of some spectral lines of an aluminum sample reached 5 J/cm^2.

The dependence of the threshold fluence F_{th} on pulse duration in the sub-picosecond regime is still not well investigated. For laser pulses with duration longer than 10 ps the value of F_{th} increases proportionally to $\sqrt{\tau_0}$ with increase of pulse duration τ_0 [32]. In many experiments it was shown that the threshold fluence dependence on pulse duration deviates from this relation for pulses with $\tau_0 < 10$ ps [33–36]. A weakening [34–36] and even reversal [33] of the $\sqrt{\tau_0}$ dependence of the threshold fluence on pulse duration were reported in the sub-picosecond regime.

In the present paper we do not make any assumptions about the nature of a target material. We choose F_{th} equal to 1.7 J/cm^2. In terms of our problem, this value corresponds to $F_{\mathrm{th}} = 10F_0$, where $F_0 = 0.17$ J/cm^2 is the initial fluence (which remains constant for all pulse durations in the case of constant energy).

Also, we assume that the value of F_{th} is the same for all of our pulses with durations $\tau_0 = 50$ fs–1 ps. Making this assumption, we take into account that due to the filamentation process all the pulses will compress in time. The difference in time scales of the compressed pulses is much smaller than those of the initial ones. Assuming a weakening of the $\sqrt{\tau_0}$ dependence of the threshold fluence for femtosecond pulses, we suppose that the difference in the F_{th} value for our pulses will be negligibly small.

Finally, we introduce HFE as the energy W_{HF} with fluence $F(r,z)$ higher than the threshold fluence F_{th}:

$$W_{\mathrm{HF}}(z) = 2\pi \int_{S_{\mathrm{HF}}} F(r,z) r\,\mathrm{d}r, \tag{7}$$

where S_{HF} is the area in the pulse cross section where the following condition is fulfilled:

$$F(r,z) \geq F_{\mathrm{th}}. \tag{8}$$

In other words, S_{HF} is the area of HFE localization.

Let us consider in detail the propagation of two pulses. The first one has $\tau_0 = 100$ fs (we will call it a 'short' pulse) and the second one has $\tau_0 = 500$ fs (we will call it a 'long' pulse). Figure 1 shows the fluence $F(r,z)$ as a function of the transverse coordinate r and propagation distance z for 'short' and 'long' pulses. The area S_{HF} where $F(r,z)$ is higher than the threshold F_{th} is marked by gray color. One can see that during pulse propagation the fluence in the surroundings of the pulse axis $F(r=0,z)$ dramatically increases. The distance z_{f} at which the fluence reaches its first maximum is very close to the filament start distance determined as the distance at which laser plasma is generated and intensity growth due to Kerr self-focusing is arrested. In what follows we will not distinguish these two distances. For a 'short' pulse the filament start distance is $z_{\mathrm{f}} = 1.4$ m. The initial intensity in a 'long' pulse is lower and the filament starts at a greater distance $z_{\mathrm{f}} = 3.8$ m.

The HFE localization area S_{HF} for each pulse has a qualitatively different form. In the case of a 'short' pulse, the fluence above threshold is localized inside several separated areas with a length of several centimeters each. In the case of a 'long' pulse, the S_{HF} area is continuous in the propagation direction and its length exceeds several meters.

Figure 2 shows HFE W_{HF} as a function of propagation distance z for pulses with different durations. One can see that the distance between areas of HFE localization, mentioned above for a 'short' pulse, is decreasing little by little with increase of pulse duration.

In our problem linear weakening of the light field is beyond consideration and the total pulse energy $W(z)$ decreases with distance only due to photoionization of air gaseous components. Figure 3 shows that pulses with shorter duration lose the same amount of energy on shorter distances. A 'short' pulse with $\tau_0 = 100$ fs loses 7% of its energy at distance $\approx$4 m, whereas a 'long' pulse with $\tau_0 = 500$ fs loses 5% of its energy only at distance $\approx$11 m.

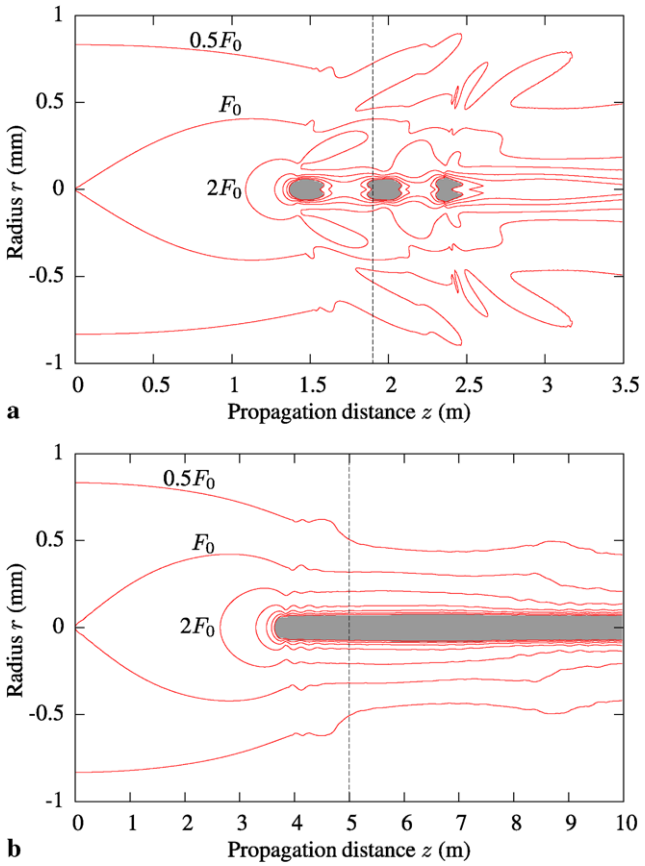

Fig. 1 Contour map of fluence $F(r,z)$ for pulses with durations $\tau_0 = 100$ fs (**a**) and $\tau_0 = 500$ fs (**b**). Here $F_0 = 0.17$ J/cm^2. Contours of $F(r,z)$ are plotted for $F = 0.5F_0, 1.0F_0, 2F_0, 4F_0, 6F_0, 8F_0, 10F_0$. Areas of HFE localization (where $F(r,z)$ is higher than the threshold fluence F_{th}) are marked by *gray color*. Energy of the pulses is 8 mJ, the beam radius is 1.2 mm. *Vertical dashed lines* mark distances z at which the intensity distribution and density of electrons are presented in Figs. 4 and 5

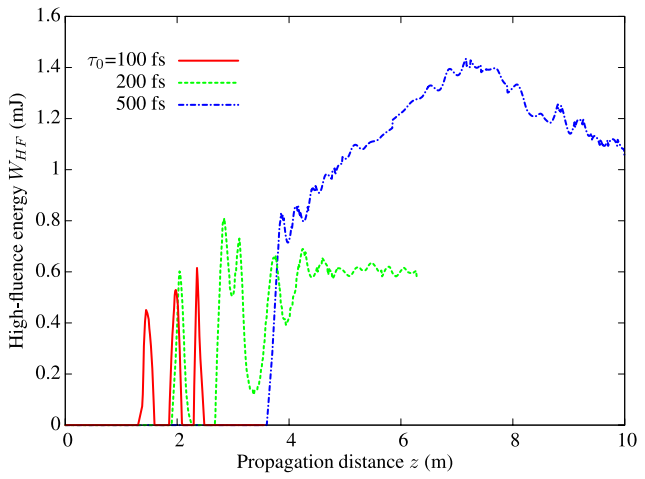

Fig. 2 High-fluence energy W_{HF} as a function of propagation distance z for pulses with different durations

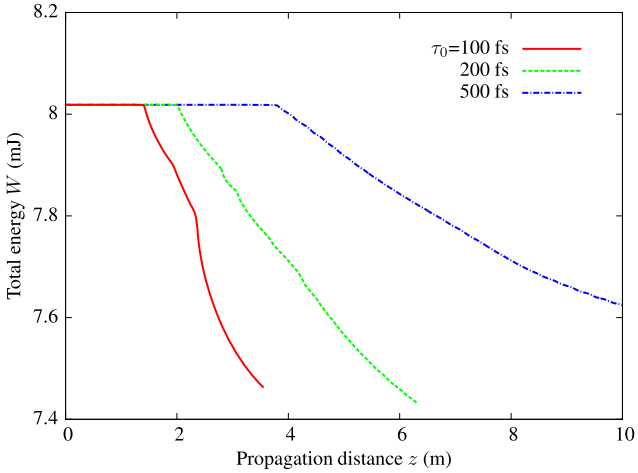

Fig. 3 Total energy W as a function of propagation distance z for pulses with different durations

To clarify the influence of an initial chirp on the HFE transport we considered two pulses with equal duration $\tau_0 = 500$ fs. The first one was transform limited, and the second one was obtained from a pulse with duration $\tau_0 = 100$ fs by applying an initial chirp. As a result we observed a difference of less than 1% in the location of the S_{HF} area border and in the value of the fluence concentrated in this area.

4 Role of pulse refocusing and plasma defocusing

For an explanation of the qualitatively different form of HFE localization areas, let us consider spatio-temporal intensity dependences in 'short' and 'long' pulses. Figure 4 illustrates temporal variations of on-axis intensity $I(r=0,z,t)$ and on-axis density of electrons $N_e(r=0,z,t)$ (see Fig. 4(a)), as well as the radial intensity distribution $I(r,z,t_i)$ for several time slices t_i (see Fig. 4(b)) of a 'short' pulse at distance $z = 1.9$ m. This distance corresponds to the beginning of the second area of HFE localization (see Fig. 1(a)). In Fig. 4(a) one can see that the nonlinear focus is shifted to the time slice $t_1 = -50$ fs of the pulse front, where a narrow peak with 5-fs duration is formed. The intensity of this peak reaches 1.6×10^{14} W/cm^2, which is higher than the air photoionization threshold. During this peak the density of electrons dramatically increases to 7.5×10^{16} cm^{-3}. The transversal intensity distribution $I(r,z,t_1)$ in the maximum of this peak has a unimodal Townes form [37] (Fig. 4(b)). Plasma generated during this intensity peak leads to defocusing of the following time slices. Energy contained in these defocusing slices is spreading out of the propagation axis. Figure 4(b) shows that due to plasma defocusing the intensity in the 'short' pulse cross section has the form of a ring structure (see plots for $t_2 = -40$ fs and $t_3 = 15$ fs time slices). In [38] it was demonstrated that ring structures in

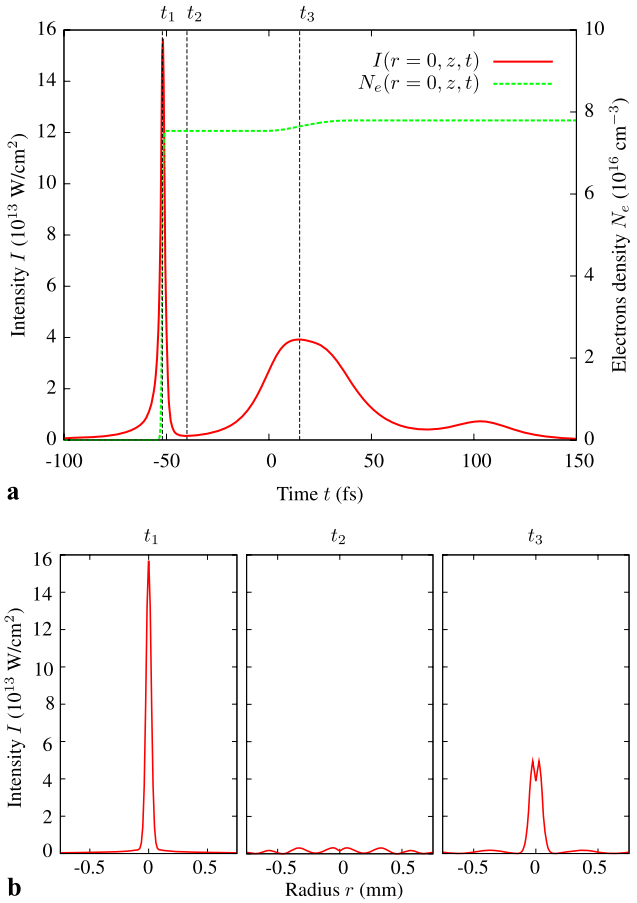

Fig. 4 Various sections of pulse with $\tau_0 = 100$ fs: (**a**) on-axis pulse shape $I(r=0,z,t)$ and on-axis electron density $N_e(r=0,z,t)$; (**b**) radial distribution of intensity $I(r,z,t_i)$ in several time slices t_i from (**a**) plot ($t_1 = -50$ fs, $t_2 = -40$ fs, $t_3 = 15$ fs). Plots correspond to the beginning of the second area of HFE at distance $z = 1.9$ m (see Fig. 1(a))

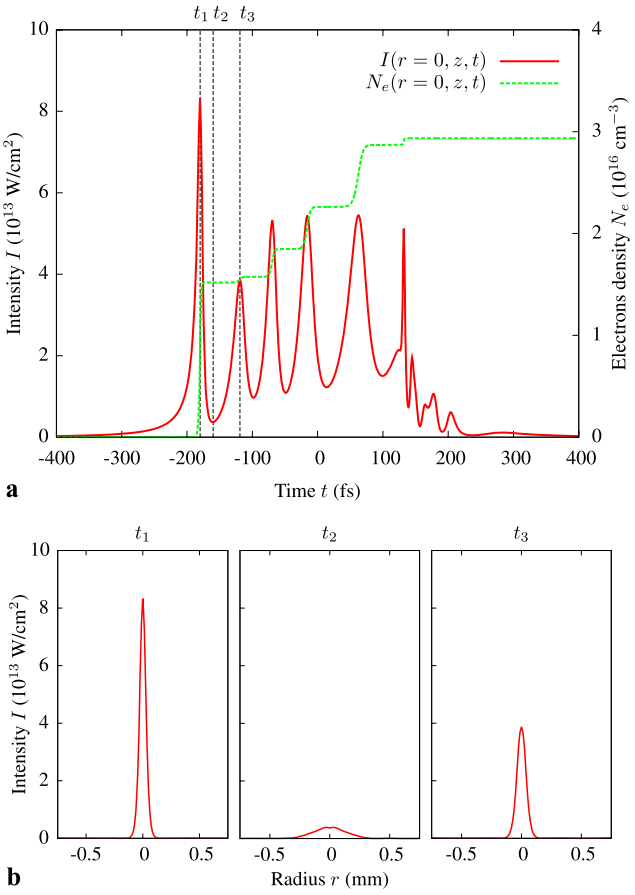

Fig. 5 Various sections of pulse with $\tau_0 = 500$ fs: (**a**) on-axis pulse shape $I(r=0,z,t)$ and on-axis electron density $N_e(r=0,z,t)$; (**b**) radial distribution of intensity $I(r,z,t_i)$ in several time slices t_i from (**a**) plot ($t_1 = -180$ fs, $t_2 = -160$ fs, $t_3 = -120$ fs). Plots correspond to the beginning of the second area of HFE at distance $z = 5$ m (see Fig. 1(b))

the pulse cross section during filamentation appear as a result of the interference of the background field and the field that diverges out from the filament's core due to the defocusing in laser plasma. In the time slice $t_3 = 15$ fs there is a second intensity maximum in the 'short' pulse temporal profile. The peak intensity of this maximum is lower than in the first one and the increment of electron density during this sub-pulse is relatively small. The same spatio-temporal dynamic can be observed in other HFE areas of the 'short' pulse.

Spatio-temporal variations in the 'long' pulse have a form which differs from the 'short' pulse case. Figure 5(a) shows the temporal variation of on-axis intensity $I(r=0,z,t)$ and electron density $N_e(r=0,z,t)$ in the HFE area ($z = 5$ m) of a 'long' pulse. The on-axis temporal shape of the 'long' pulse contains a sequence of multiple peaks. The first peak is formed due to focusing of undistorted time slices. All following peaks are formed due to multiple refocusing in slices defocused by plasma. The intensity in the first peak ($t_1 = -180$ fs) reaches 8×10^{13} W/cm^2 and the electron density reaches 1.5×10^{16} cm^{-3}. These values are smaller than in the case of the 'short' pulse. One should note that in comparison with the 'short' pulse, where electrons are generated mainly by the first maximum of the intensity, here each intensity peak formed due to the refocusing gives rise to a considerable increment of electron density. At the end of the pulse the on-axis density of electrons reaches 2.8×10^{16} cm^{-3}. The transversal intensity distribution in the first peak has a unimodal Townes profile like in the 'short' pulse. The duration of this first peak is 20 fs, which is greater than the 5-fs duration of the first peak in the case of the 'short' pulse. As in the case of the 'short' pulse, following temporal slices propagate in ionized air and undergo plasma defocusing. But, the radial distribution of intensity $I(r,z,t)$ in these slices stays unimodal (see slices $t_2 = -160$ fs and $t_3 = -120$ fs in Fig. 5(b)). There is no ring structure in the cross section of the 'long' pulse temporal slices involved in defocusing. In order to explain the absence of defocus-

Table 1 Parameters of filaments and plasma channels for pulses with different durations τ_0 and constant initial energy W_0. P_0/P_{cr}—ratio of initial pulse power P_0 to self-focusing critical power P_{cr}; I_0—initial pulse intensity; F_0—initial pulse fluence; z_f—distance of filament start; I_{fil}, F_{fil}—filament intensity and fluence determined at z_f; r_{pl}, N_e, D_e—plasma channel radius, density of electrons, and linear density determined at z_f; $\overline{R}_{HF}$—average radius of HFE localization area; $\overline{W}_{HF}$—average value of HFE transported by filament; Q—efficiency of HFE transport determined by (10)

τ_0 fs	W_0 mJ	P_0/P_{cr}	I_0 10^{12} W/cm^2	F_0 J/cm^2	z_f m	I_{fil} 10^{13} W/cm^2	F_{fil} J/cm^2	r_{pl} μm	N_e 10^{16} cm^{-3}	D_e 10^{13} m^{-1}	$\overline{R}_{HF}$ μm	$\overline{W}_{HF}$ mJ	Q %
50	8	38.0	2.00	0.17	1.0	9.9	2.2	22.4	5.96	9.0	59	0.22	2.7
100	8	19.0	1.00	0.17	1.4	8.4	4.3	22.1	5.78	8.8	62	0.32	4.0
200	8	9.5	0.50	0.17	2.0	7.4	6.8	21.1	5.76	8.2	65	0.42	5.2
300	8	6.3	0.33	0.17	2.6	7.0	8.4	19.8	5.63	7.5	75	0.60	7.5
500	8	3.8	0.20	0.17	3.8	6.3	10.5	19.2	4.68	5.4	86	1.13	14.1
750	8	2.5	0.13	0.17	5.6	5.4	12.1	16.9	3.07	3.2	89	1.24	15.5
1000	8	1.9	0.10	0.17	7.8	4.4	12.3	17.2	1.70	1.7	92	1.28	16.0

ing rings in the case of the 'long' pulse, one can note that because of the constant energy of both pulses the P_0/P_{cr} ratio of the 'long' pulse is five times less than that of the 'short' one. Therefore, Kerr self-focusing of the 'long' pulse is 'softer'. As a result, less plasma is needed to stop intensity growth. That is what we see for the density of electrons generated by the first intensity peak: 1.5×10^{16} cm^{-3} for the 'long' pulse versus 7.5×10^{16} cm^{-3} for the 'short' pulse. The smaller amount of plasma generated by the first peak makes defocusing in it less strong. Smaller defocusing leads to less energy spread out of the beam axis, which results in formation of a continuous HFE channel.

For a quantitative description of HFE transport by a filament, we use the average value of HFE $\overline{W}_{HF}$ determined by the equation

$$\overline{W}_{HF} = \frac{\int_{L_{HF}} W_{HF}(z)\,dz}{\int_{L_{HF}} dz}, \tag{9}$$

where L_{HF} is the length of the HFE localization area along the z axis (three spots for 'short' pulse and continuous area for 'long' pulse in Fig. 1). The efficiency Q of HFE transport will be expressed as the ratio of $\overline{W}_{HF}$ to the initial pulse energy W_0 expressed in percent:

$$Q = \frac{\overline{W}_{HF}}{W_0} \times 100\%. \tag{10}$$

Parameters of the filament and plasma channel in pulses with different durations are summarized in Table 1. The submitted data shows that in the case of constant energy, pulses with greater duration form filaments with lower intensity I_{fil} but higher fluence F_{fil}. The average radius $\overline{R}_{HF}$ of the S_{HF} area (where high fluence is localized) increases with increase of pulse duration. A filament of a pulse with greater duration has higher average HFE $\overline{W}_{HF}$ in comparison with a pulse of lower duration. The efficiency of HFE transport

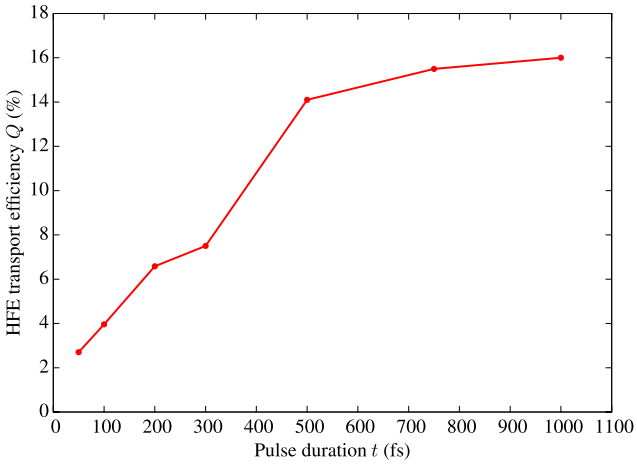

Fig. 6 Efficiency of HFE transport Q as a function of pulse duration τ_0

Q increases with growth of pulse duration. Increase of pulse duration in the case of constant energy leads to decrease of electron density N_e and radius of the plasma channel r_{pl}. This results in a significant decrease of the linear density of electrons $D_e = 2\pi \int N_e(r,z) r\,dr$.

Figure 6 shows the efficiency of HFE transport Q as a function of pulse duration. The efficiency Q increases by several times with an increase of the pulse duration τ_0 from 100 to 500 fs and saturates during a further increase of τ_0. Saturation of Q with an increase of τ_0 is what one can expect. If one increases the pulse duration and keeps the energy constant then at some point the initial peak power will be less than the self-focusing critical power and there will be no HFE transport at all.

Parameters of filaments and plasma channels are explained by the nature of Kerr self-focusing determined by pulse energy and duration. In the case of constant energy in the pulses, the ratio of the initial power to the critical one P_0/P_{cr} decreases with longer pulse duration, and self-

Table 2 Parameters of filaments and plasma channels for pulses with different durations τ_0 and constant initial ratio of initial pulse power P_0 to self-focusing critical power P_{cr}. W_0—initial pulse energy; I_0—initial pulse intensity; F_0—initial pulse fluence; z_f—distance of filament start; I_{fil}, F_{fil}—filament intensity and fluence determined at z_f; r_{pl}, N_e, D_e—plasma channel radius, density of electrons, and linear density determined at z_f; $\overline{R}_{HF}$—average radius of HFE localization area; $\overline{W}_{HF}$—average value of HFE transported by filament; Q—efficiency of HFE transport determined by (10)

τ_0 fs	W_0 mJ	P_0/P_{cr}	I_0 10^{12} W/cm^2	F_0 J/cm^2	z_f m	I_{fil} 10^{13} W/cm^2	F_{fil} J/cm^2	r_{pl} μm	N_e 10^{16} cm^{-3}	D_e 10^{13} m^{-1}	$\overline{R}_{HF}$ μm	$\overline{W}_{HF}$ mJ	Q %
50	4	19	1	0.09	1.6	10.1	1.9	20.3	5.31	7.0	34	0.05	1.4
100	8	19	1	0.17	1.4	8.4	4.3	22.1	5.78	8.8	62	0.32	4.0
200	16	19	1	0.35	1.3	7.6	7.4	23.2	6.98	11.2	89	0.84	9.7
500	40	19	1	0.89	1.2	6.8	13.2	22.2	8.39	12.6	219	4.90	12.2

focusing becomes less sharp. Under such conditions dynamical equilibrium of Kerr compression and plasma defocusing is reached for a smaller density of electrons. Vice versa, with an increase of the P_0/P_{cr} ratio the Kerr lens becomes tight and strong plasma defocusing is needed to stop the intensity growth. During such defocusing, energy goes out to the periphery of the pulse cross section and Kerr nonlinearity cannot localize it on the axis again. As a result, the number of refocusing cycles and the amount of HFE transported by the filament decrease.

Growth of HFE transported by the filament with an increase of pulse duration takes place in the case of constant P_0/P_{cr} ratio, too (see Table 2). The initial energy W_0 of pulses with constant P_0/P_{cr} ratio increases with an increase of pulse duration.

In pulses with constant P_0/P_{cr} ratio, with increase of duration the time interval containing time slices which undergo refocusing increases. Therefore, in pulses with constant P_0/P_{cr}, the W_{HF} value increases considerably with increase of duration. Table 2 contains the average value of W_{HF}, which is determined by (7) for $F_{th} = 1.7$ J/cm^2. Efficiency of energy transformation to HFE during filamentation of pulses with constant P_0/P_{cr} ratio also increases with increase of duration.

However, in contrast to the case of constant W_0, an increase of pulse duration in the case of constant P_0 results in an increase of electron density N_e and D_e. At that time, the intensity in the filament I_{fil} decreases. This is the evidence that in pulses with higher duration generation of plasma takes place during a longer time period.

Note that in the case of constant initial power P_0 an increase of pulse duration leads to an insignificant growth of the optical strength of Kerr self-focusing due to the growth of the Raman scattering contribution to the increment of the refractive index Δn_k (see (2)). Therefore, the filament start distance decreases (see Table 2). This effect is especially strong for pulses with longer duration.

5 Conclusions

We showed that an increase of pulse duration leads to higher efficiency of HFE localization during filamentation in both cases of constant energy W_0 and constant power P_0. This is due to the fact that the parameters of filaments and plasma channels of femtosecond laser pulses in air depend on the strength (sharpness) of Kerr focusing. In pulses with peak power $P_0 \leq 4P_{cr}$ the Kerr phase shift is quite small and dynamical equilibrium of self-focusing and plasma defocusing is reached for a small density of electrons $N_e \leq 4.6\times10^{16}$ cm^{-3}. Under these conditions plasma defocusing is mostly aberrationless. Laser energy remains in an area close to the beam axis. As a result of multiple refocusing in the filament, a continuous area of high fluence is formed. The total amount of HFE transported by the filament reaches 14% of the initial pulse energy. In the case of tight Kerr focusing of a pulse with $P_0 \geqslant 10P_{cr}$, the density of electrons in the induced plasma reaches $N_e \approx 10^{17}$ cm^{-3} and defocusing inside this plasma is aberrational with formation of ring structures in the intensity distribution. Divergent rings carry out energy to the periphery of the pulse cross section. Several separated areas with high fluence are formed. Inside these areas there is HFE which is less than 5% of the total energy.

Finally, we can conclude that one can expect that pulses with greater duration are more suitable for filament-induced breakdown spectroscopy of remote targets.

In our further investigations we will try to make the generalization of the formulated conclusions to the case of multifilamentation of powerful femtosecond laser pulses under real atmospheric conditions.

Acknowledgement This work has been funded by the Russian Federal Agency for Science and Innovations (Rosnauka) under the state contract 02.740.11.0223.

References

1. S.L. Chin, S.A. Hosseini, W. Liu, Q. Luo, F. Theberge, N. Aközbek, A. Becker, V.P. Kandidov, O. Kosareva, H. Schroeder, Can. J. Phys. **83**, 863 (2005)
2. A. Couairon, A. Mysyrowicz, Phys. Rep. **441**(2–4), 47 (2007)
3. V.P. Kandidov, S.A. Shlenov, O.G. Kosareva, Quantum Electron. **39**(3), 205 (2009)
4. J. Kasparian, M. Rodriguez, G. Mejean, J. Yu, E. Salmon, H. Wille, R. Bourayou, S. Frey, Y.-B. André, A. Mysyrowicz, R. Sauerbrey, J.-P. Wolf, L. Wöste, Science **301**(5629), 61 (2003)
5. J. Kasparian, J.-P. Wolf, Opt. Express **16**(1), 466 (2008)
6. S.L. Chin, H.L. Xu, Q. Luo, F. Théberge, W. Liu, J.-F. Daigle, Y. Kamali, P.T. Simard, J. Bernhardt, S.A. Hosseini, M. Sharifi, G. Méjean, A. Azarm, C. Marceau, O.G. Kosareva, V.P. Kandidov, N. Aközbek, A. Becker, G. Roy, P. Mathieu, P.T. Simard, M. Châteauneuf, J. Dubois, Appl. Phys. B: Lasers Opt. **95**, 1 (2009)
7. J. Kasparian, R. Sauerbrey, S.L. Chin, Appl. Phys. B: Lasers Opt. **71**, 877 (2000)
8. Q. Luo, H.L. Xu, S.A. Hosseini, J.-F. Daigle, F. Théberge, M. Sharifi, S.L. Chin, Appl. Phys. B: Lasers Opt. **82**, 105 (2006)
9. G. Méjean, J. Kasparian, J. Yu, S. Frey, E. Salmon, J.-P. Wolf, Appl. Phys. B: Lasers Opt. **78**, 535 (2004)
10. J.-F. Daigle, G. Méjean, W. Liu, F. Théberge, H.L. Xu, Y. Kamali, J. Bernhardt, A. Azarm, Q. Sun, P. Mathieu, G. Roy, J.-R. Simard, S.L. Chin, Appl. Phys. B: Lasers Opt. **87**, 749 (2007)
11. O. Kosareva, N.A. Panov, N. Aközbek, V.P. Kandidov, Q. Luo, S.A. Hosseini, W. Liu, J.-F. Gravel, G. Roy, S.L. Chin, Appl. Phys. B: Lasers Opt. **82**, 111 (2006)
12. Z. Jin, J. Zhang, M.H. Xu, X. Lu, Y.T. Li, Z.H. Wang, Z.Y. Wei, X.H. Yuan, W. Yu, Opt. Express **13**(25), 10424 (2005)
13. P. Rohwetter, K. Stelmaszczyk, L. Wöste, R. Ackermann, G. Méjean, E. Salmon, J. Kasparian, J. Yu, J.-P. Wolf, Spectrochim. Acta Part B: At. Spectrosc. **60**, 1025 (2005)
14. N.T. Nguyen, A. Saliminia, W. Liu, S.L. Chin, R. Vallée, Opt. Lett. **28**(17), 1591 (2003)
15. K. Stelmaszczyk, P. Rohwetter, G. Méjean, J. Yu, E. Salmon, J. Kasparian, R. Ackermann, J.-P. Wolf, L. Wöste, Appl. Phys. Lett. **85**(18), 3977 (2004)
16. H.L. Xu, J. Bernhardt, P. Mathieu, G. Roy, S.L. Chin, J. Appl. Phys. **101**(3), 033124 (2007)
17. O.G. Kosareva, V.P. Kandidov, A. Brodeur, C.-Y. Chien, S.L. Chin, Opt. Lett. **22**(17), 1332 (1997)
18. A. Chiron, B. Lamouroux, R. Lange, J.-F. Ripoche, M. Franco, B. Prade, G. Bonnaud, G. Riazuelo, A. Mysyrowicz, Eur. Phys. J. D, At. Mol. Opt. Plasma Phys. **6**, 383 (1999)
19. S.A. Akhmanov, V.V. Vysloukh, A.S. Chirkin, *Optics of Femtosecond Laser Pulses* (American Institute of Physics, New York, 1992)
20. T. Brabec, F. Krausz, Phys. Rev. Lett. **78**, 3282 (1997)
21. P.A. Oleinikov, V.T. Platonenko, Laser Phys. **3**(3), 618 (1993)
22. E.T.J. Nibbering, G. Grillon, M.A. Franco, B.S. Prade, A. Mysyrowicz, J. Opt. Soc. Am. B **14**(3), 650 (1997)
23. J.-F. Ripoche, G. Grillon, B. Prade, M. Franco, E. Nibbering, R. Lange, A. Mysyrowicz, Opt. Commun. **134**(4), 310 (1997)
24. M. Mlejnek, E.M. Wright, J.V. Moloney, Opt. Lett. **23**(5), 382 (1998)
25. A.M. Perelomov, V.S. Popov, M.V. Terent'ev, Sov. Phys. JETP **23**(5), 924 (1966)
26. A. Talebpour, J. Yang, S.L. Chin, Opt. Commun. **163**, 29 (1999)
27. M. Mlejnek, M. Kolesik, J.V. Moloney, E.M. Wright, Phys. Rev. Lett. **83**(15), 2938 (1999)
28. J. Krüger, W. Kautek, Laser Phys. **9**(1), 30 (1999)
29. P. Rohwetter, J. Yu, G. Méjean, K. Stelmaszczyk, E. Salmon, J. Kasparian, J.-P. Wolf, L. Wöste, J. Anal. At. Spectrom. **19**, 437 (2004)
30. M. Lenzner, J. Krüger, S. Sartania, Z. Cheng, C. Spielmann, G. Mourou, W. Kautek, F. Krausz, Phys. Rev. Lett. **80**, 4076 (1998)
31. B. Le Drogoff, F. Vidal, Y. von Kaenel, M. Chaker, T.W. Johnston, S. Laville, M. Sabsabi, J. Margot, J. Appl. Phys. **89**(12), 8247 (2001)
32. J.P. Singh, S.N. Thakur (eds.), *Laser Induced Breakdown Spectroscopy* (Elsevier, Amsterdam, 2007)
33. D. Du, X. Liu, G. Korn, J. Squier, G. Mourou, Appl. Phys. Lett. **64**(23), 3071 (1994)
34. B.C. Stuart, M.D. Feit, A.M. Rubenchik, B.W. Shore, M.D. Perry, Phys. Rev. Lett. **74**, 2248 (1995)
35. B.C. Stuart, M.D. Feit, S. Herman, A.M. Rubenchik, B.W. Shore, M.D. Perry, J. Opt. Soc. Am. B **13**(2), 459 (1996)
36. A.-C. Tien, S. Backus, H. Kapteyn, M. Murnane, G. Mourou, Phys. Rev. Lett. **82**, 3883 (1999)
37. R.Y. Chiao, E. Garmire, C.H. Townes, Phys. Rev. Lett. **13**, 479 (1964)
38. S.L. Chin, S. Petit, W. Liu, A. Iwasaki, M.-C. Nadeau, V.P. Kandidov, O.G. Kosareva, K.Y. Andrianov, Opt. Commun. **210**(3–6), 329 (2002)